Biochemical Journal (2021) **478** 1749–1767
https://doi.org/10.1042/BCJ20210117

PORTLAND PRESS

Research Article

Structures of an engineered phospholipase D with specificity for secondary alcohol transphosphatidylation: insights into plasticity of substrate binding and activation

Ariela Samantha[1], Jasmina Damnjanović[2], Yugo Iwasaki[2], Hideo Nakano[2] and Alice Vrielink[1]

[1]School of Molecular Sciences, University of Western Australia, 35 Stirling Highway, Crawley, WA 6009, Australia; [2]Laboratory of Molecular Biotechnology, Graduate School of Bioagricultural Sciences, Nagoya University, Furo-cho, Chikusa-ku, Nagoya 464-8601, Japan

Correspondence: Alice Vrielink (alice.vrielink@uwa.edu.au)

Phospholipase D (PLD) is an enzyme useful for the enzymatic modification of phospholipids. In the presence of primary alcohols, the enzyme catalyses transphosphatidylation of the head group of phospholipid substrates to synthesise a modified phospholipid product. However, the enzyme is specific for primary alcohols and thus the limitation of the molecular size of the acceptor compounds has restricted the type of phospholipid species that can be synthesised. An engineered variant of PLD from *Streptomyces antibioticus* termed TNYR SaPLD was developed capable of synthesising 1-phosphatidylinositol with positional specificity of up to 98%. To gain a better understanding of the substrate binding features of the TNYR SaPLD, crystal structures have been determined for the free enzyme and its complexes with phosphate, phosphatidic acid and 1-inositol phosphate. Comparisons of these structures with the wild-type SaPLD show a larger binding site able to accommodate a bulkier secondary alcohol substrate as well as changes to the position of a flexible surface loop proposed to be involved in substrate recognition. The complex of the active TNYR SaPLD with 1-inositol phosphate reveals a covalent intermediate adduct with the ligand bound to H442 rather than to H168, the proposed nucleophile in the wild-type enzyme. This structural feature suggests that the enzyme exhibits plasticity of the catalytic mechanism different from what has been reported to date for PLDs. These structural studies provide insights into the underlying mechanism that governs the recognition of *myo*-inositol by TNYR SaPLD, and an important foundation for further studies of the catalytic mechanism.

Introduction

Phospholipids (PLs) are important biological molecules that play critical roles in the maintenance of cell membrane integrity as well as participating in a number of metabolic processes [1,2]. They are also used as food additives, in drug delivery systems and as emulsifying agents in various products such as nutraceuticals and pharmaceuticals. To obtain highly pure PLs, commercially available mixtures obtained by extraction from plant sources require purification steps or chemical modifications to introduce homogeneity in terms of fatty acid and head group composition. Alternatively, they can be obtained via chemical synthetic routes which have poor cost and yield performance and require the use of environmentally toxic reagents.

Phospholipases are a large family of enzymes that act on PL substrates and can be utilised in the industrial production of phospholipids by enzymatic or semi-synthetic methods. Phospholipase D (PLD) (EC 3.1.4.4) hydrolyses the terminal phosphodiester bond, releasing phosphatidic acid (PA)

Received: 1 March 2021
Revised: 6 April 2021
Accepted: 9 April 2021

Accepted Manuscript online: 12 April 2021
Version of Record published: 10 May 2021

PORTLAND PRESS

Biochemical Journal (2021) **478** 1749–1767
https://doi.org/10.1042/BCJ20210117

and the polar head group. PA is a lipid secondary messenger, thus PLD belongs to a superfamily of signalling enzymes. In addition to hydrolysis, PLD uniquely catalyses transphosphatidylation in the presence of primary alcohols, releasing a head group alcohol and a new phospholipid modified at the polar head [1,3]. The catalytic activity is supported by the residues of the HxKxxxxDx6GSxN (HKD) motif which appears twice in the protein sequence and forms a symmetrical active site. The reaction proceeds by a two-step S_N2-type nucleophilic substitution with the formation of a covalently bound phosphatidyl-enzyme intermediate [4,5], where the function of the nucleophile and general acid/general base is performed by the two histidine residues.

Among PLDs from various sources, *Streptomyces* sp. PLDs display the highest transphosphatidylation activity [6–8] and, as a result, have become the most commonly employed enzymes for the syntheses of unnatural or low-abundance PLs from abundantly available phosphatidylcholine (reviewed in [9]). The reaction also provides the possibility of modifying the polar head of PLs with various bioactive compounds, and therefore the phosphatidyl moiety of PLs can be utilised as a biocompatible carrier for the delivery of bioactive compounds. However, utilisation of PLD for the synthesis of bioactive PLs was limited by the specificity of transphosphatidylation towards primary alcohols, and thus the molecular size and bulkiness of the acceptor compounds by the enzyme. For example, synthesis of phosphatidylinositol (PI) using PLD was not possible since *myo*-inositol, a fully hydroxylated cyclohexanol, could not be accommodated as an acceptor compound by the enzyme. To overcome the limitations of PLD's transphosphatidylation, protein engineering techniques were utilised to alter the substrate specificity of PLD from *Streptomyces antibioticus* (SaPLD) to accept *myo*-inositol [10–12]. *Myo*-inositol is the most abundant stereoisomer of inositol in nature included in the structure of PI and all phosphoinositides, and thus was chosen as the substrate.

The protein engineering efforts towards obtaining a PLD with an active site able to accept *myo*-inositol, have started with site-directed saturation mutagenesis of three residues in the active site of SaPLD, W187, Y191 and Y385, believed to affect acceptor accommodation and binding. As a result, 25 SaPLD mutants have been isolated with PI-synthesising activity [10]. However, the isolated variants had low positional specificity, i.e. reacted on multiple hydroxyls of *myo*-inositol instead of 1-OH only, which would yield 1-PI, the only natural PI isomer. To tune the positional specificity of engineered PLD towards 1-OH of *myo*-inositol, a second round of site-directed mutagenesis was initiated targeting residue 187, while keeping the residue 191 as Y and 385 as R. The choice of residue 187 as a mutation target was made after observing that the mutants which showed the highest specificity in 1-PI synthesis all had Y at position 191 and R at position 385. Among 65 newly isolated PI-synthesising SaPLDs from this round of mutagenesis, the best performing variants were identified as NYR (187N) and HYR (187H) [11,13], and showed positional specificity of >60%. To gain further improvement, the third and final round of mutagenesis has been performed by separately targeting another four residues of the substrate-binding site of NYR SaPLD. The best performing variant, TNYR incorporated a G186T mutation and showed positional specificity of up to 98% [12]. Besides *myo*-inositol, two first-generation mutant SaPLDs, namely KWY and FYL, were found to accept other bulky substrates, such as β-D-glucose and L-threonine, respectively, and catalyse the synthesis of 1-phosphatidyl-β-D-glucose and phosphatidylthreonine [14,15]. Based on these findings, we believe that the mutations in the first generation expanded the active site while the mutations in the second and third generation of SaPLD mutants contributed to the positional specificity towards 1-PI. To better understand the molecular details for substrate binding and to probe the mechanism that enables the enzymatic synthesis of 1-PI, crystallographic studies of the TNYR variant of SaPLD were undertaken.

Materials and methods

Protein expression and purification

Recombinant protein expression was carried out using *E. coli* strain BL21(DE3) transformed with the pETKmS1-Term vector harbouring the gene of TNYR SaPLD, as reported previously [12]. Pre-culture in LB medium containing 50 μg/ml kanamycin grown at 37°C with shaking for 12 h was used to inoculate the main culture consisting of a defined-expression medium [16] where gene expression was triggered by autoinduction [17]. Cells were cultured at 30°C with shaking for 72 h. TNYR SaPLD is mainly expressed as an extracellular protein due to the presence of the *pelB* signal sequence upstream of the *pld* gene. Therefore, after the cultivation, the culture was centrifuged at 8500×***g*** and 4°C for 20 min to remove the bacterial cells and recover the culture supernatant which was used for PLD isolation by ammonium sulfate precipitation at 90% saturation.

The precipitated TNYR SaPLD was recovered by centrifugation at 8500×***g*** and 4°C for 60 min. The protein precipitate was gently resuspended in ∼60 ml double distilled water (ddH2O). The resuspended crude PLD

Biochemical Journal (2021) 478 1749–1767
https://doi.org/10.1042/BCJ20210117

solution was then dialysed against 50 mM sodium acetate pH 5.0 at 4°C overnight to precipitate out protein contaminants through a low pH precipitation procedure. The insoluble protein contaminants were removed from the solution by centrifugation at 3300×***g*** and 4°C for 30 min. The supernatant solution containing crude PLD was then dialysed at 4°C overnight against 20 mM Tris–HCl pH 8.0, centrifuged at 3300×***g*** and 4°C for 30 min and passed through 0.4 μm filter to remove any precipitated protein contaminants in preparation for fast performance liquid chromatography (FPLC). As the mutant protein did not contain an affinity tag, a series of chromatography steps were required to obtain highly pure material suitable for crystallisation experiments. Four consecutive chromatography steps were used in the purification process: (1) anion exchange chromatography (5 ml HiTrap Q FF column, GE Healthcare; gradient elution with NaCl in 20 mM Tris–HCl pH 8.0 buffer), (2) affinity chromatography (5 ml Maltose-Binding-Protein/MBPTrap HP column, GE Healthcare; isocratic elution with 150 mM NaCl in 20 mM Tris–HCl pH 8.0 buffer), (3) cation exchange chromatography (1 ml HiTrap CM FF column, GE Healthcare; gradient elution with NaCl in 50 mM acetate buffer pH 5.0) and (4) size exclusion chromatography (HiLoad Superdex75 16/60 column, GE Healthcare; isocratic elution with 150 mM NaCl in 20 mM Tris–HCl pH 8.0 buffer). All chromatographic steps were performed on the FPLC Äkta™ Design System at 4°C. An MBPTrap column was used to remove the *E. coli* maltodextrin-binding protein which was a major contaminant in the PLD purification process.

The fractions containing pure SaPLD were pooled and dialysed against 10 mM Tris–HCl pH 8.0. Pure protein fractions as assessed by SDS–PAGE were concentrated to 15–18 mg/ml as determined by the absorbance at 280 nm using a calculated molar extinction coefficient for the SaPLD TNYR mutant (74 870 M^{-1} cm^{-1}) and used for crystallization experiments.

Protein crystallization

Screening of crystallisation conditions for the TNYR SaPLD mutant was carried out starting with the known crystallisation condition of wild-type (WT) SaPLD, which was 15% polyethylene glycol MWt-6000 (PEG6K) and 100 mM 2-(*N*-morpholinoethanesulfonic acid (MES) buffer pH 6.0. The screening was conducted by the hanging drop vapour diffusion method using VDX 24-well plates. Lead conditions from the initial screens were further optimised using the Additive Screen Kit (Hampton Research). Optimised crystallisation drops contained 1 μl protein, 1 μl crystallisation solution (14 to 22% (w/v) PEG6K and 100 mM MES pH 4.0–4.8), and 0.2 μl 5% (w/v) lauryldimethylamine *N*-oxide (LDAO). Drops were equilibrated at 20°C against 1 ml crystallisation solution in the reservoir. Needle cluster-like crystals appeared within ∼7 days.

Preparation of 1-inositol phosphate

1-inositol phosphate was prepared enzymatically from 50% crude PI in the bi-phasic reaction with *Streptomyces antibioicus* PI-specific phospholipase C1 (PI-PLC1) [18]. The reaction consisted of an organic solvent phase including 2 ml of diethyl ether and 500 μl of ethanol in which 250 mg of PI was dissolved. The water phase consisted of 2.25 ml of 20 mM Tris–HCl pH 7.2 containing 10 μM $CaCl_2$ and 62.5 μg of SaPI-PLC1. Four vials with the above reaction mixture composition were set and incubated at 30°C for 24 h with shaking. After 24 h, 10 ml of water, 125 μl of 2 N HCl and 10 ml of chloroform/ methanol = 2/1 were added to each vial to quench the reaction and extract remaining phospholipids and PI. After the separation of organic and water layers, TLC analysis was performed to analyse the composition of each phase. The organic phase was spotted onto a silica-coated plate, developed in chloroform:methanol:petroleum ether:acetic acid (4 : 2 : 3 : 1), and detected with Dittmer-Lester reagent. The water phase was spotted onto a cellulose-coated plate, developed in 1-propanol:water:acetic acid (5 : 4 : 1), and detected with Hannes-Isherwood reagent. Hydrolysis of PI to 1-inositol phosphate was confirmed by the absence of PI spot in the organic phase and detection of a single spot on the cellulose-coated TLC plate (Supplementary Figure S1). The water phase containing the 1-inositol phosphate was then passed through a cation exchange resin (Dowex Marathon C-10 Na^+, Fujifilm, Japan) washed with water, to remove the calcium ions. After the confirmation of product recovery in the eluted fraction, the solution was freeze-dried, and used for the crystallographic experiments.

Crystal soaking and co-crystallisation with substrates or 1-inositol phosphate

Soak and co-crystal methods were undertaken to obtain the protein in complex with ligands. Co-crystallization of the protein with monopotassium phosphate and *myo*-inositol was carried out by dissolving both ligands in the protein buffer (10 mM Tris–HCl pH 8.0). The dissolved ligand mixture was added to the protein solution at a final concentration of 20 mM for each ligand followed by incubation of the mixture on ice for 1 h.

PORTLAND PRESS

Biochemical Journal (2021) **478** 1749–1767
https://doi.org/10.1042/BCJ20210117

Co-crystallisation of the protein with 1-inositol phosphate was carried out by dissolving 1-inositol phosphate in the protein buffer. The dissolved ligand was added to the protein solution at a final concentration of 10 mM and the mixture was incubated on ice for 1 h. The protein-ligand mixture was then used in fresh crystallisation droplets as described above.

For soaking experiments, crystals were transferred to a new drop of artificial reservoir solution which contained the substrate (2 mM diC_4PC) or product analogue (5 mM 1-inositol phosphate). For these soaks the artificial mother liquor was typically 1% higher in PEG6K concentration than that used for the crystal growth. The drops were placed over a well and incubated at 20°C for different soak times.

X-ray structure determination

Single crystals were transferred briefly to a droplet containing the artificial reservoir solution and 20% (w/v) glycerol as cryo-protectant and then mounted on a nylon loop and flash frozen in liquid nitrogen. Diffraction data collection was carried out at the Australian Synchrotron beamlines MX1 and MX2. The MX1 beamline was equipped with an ADSC Quantum 210r CCD detector and the MX2 beamline was equipped with an EIGER X 16M pixel detector with continuous readout ('shutterless' data collection). All data were collected using 180 or 360° of crystal rotation. Diffraction data were integrated using the XDS processing package [19] and data reduction and structure solution carried out using the CCP4 software package [20]. The structure was solved by the molecular replacement method with the program PHASER using the WT SaPLD (PDB: 2ZE4) as the search model [21]. Cycles of model building and crystallographic refinement were carried out using the COOT and PHENIX software suite, respectively. The final data reduction and refinement statistics are given in Table 1.

Results

Overall description of the TNYR SaPLD structure

Crystals of the unliganded TNYR SaPLD diffracted to 2.49 Å resolution at the MX2 beamline at the Australian Synchrotron. The structure was solved by the molecular replacement method using PHASER MR within the CCP4 suite of crystallographic software [20]. WT SaPLD (PDB: 2ZE4) was used as the search model for the molecular replacement method. All data reduction and structure refinement statistics are provided in Table 1. As expected, the structure adopts a monomeric bilobed domain arrangement with a pseudo-dimeric architecture, composed of an N-terminal lobe and a C-terminal lobe (Figure 1A). The pseudo-dimeric architecture is the hallmark of the monomeric proteins from the PLD superfamily containing an HKD catalytic motif [6]. The overall structure of the TNYR SaPLD is similar to PLD from *Streptomyces* strain PMF (PMF PLD; PDB: 1V0S) [22,23] which adopts a α-β-α-β sandwich with overall dimensions of ~72 Å × 52 A˚ × 46 A˚. TNYR SaPLD consists of 13 α-helices and 2 β-sheets. The β-sheets form a β-sandwich fold at the interface of the two lobes. The 13 α-helices flank the β-sandwich fold, with two long helices running diagonally along the inner surface of each β-sheet. These two diagonal helices are thought to provide the necessary framework for keeping the active site in an open and accessible conformation for substrate entry [23]. Several flexible loops are found at the interface of the lobes, surrounding the conserved catalytic HKD-motifs which might contribute to the broad substrate specificity of SaPLD. The conserved catalytic residues are H168 and H442, K170 and K444, and N185 and N459, respectively, for each lobe and are located on the loops, near to each other. The residues D200 and D467 which coordinate the catalytic histidine residues by hydrogen bond contacts are also found on the loops (Figure 1B).

The active site of the enzyme contains two bound water molecules that make hydrogen bonds with the catalytic histidine (H168 and H442), lysine (K170 and K444) and asparagine (N185 and N459) residues (Supplementary Figure S2).

Distinctive features of the TNYR SaPLD structure

Three residues had been mutated relative to the WT enzyme: G186 (mutated to T), W187 (mutated to N), and Y385 (mutated to R), while Y191 remained unchanged. The densities for the side-chains of these residues are clearly visible in the structure confirming their presence. The N187 side-chain faces the exterior of the structure ($\chi_1 = -175°$), unlike the W187 in the WT structure ($\chi_1 = -63°$) directed inwards, towards the active site region (Figure 2A,B). The asparagine side-chain makes a hydrogen bond contact to the main-chain of D189. This smaller side-chain and different orientation results in the formation of a larger binding pocket compared with the WT structure which may enable a bulkier substrate such as *myo*-inositol to bind to the enzyme (Figure 2A,B). Indeed, analysis of the topographic features of the TNYR variant in comparison with the WT protein using the

Biochemical Journal (2021) **478** 1749–1767
https://doi.org/10.1042/BCJ20210117

Table 1 Crystallographic data collection and refinement statistics

Protein	***TNYR***						***H168A TNYR***
Ligand	-	Phosphate/ *myo*-inositol	diC_4PC	diC_4PC	diC_4PC	1-Inositol Phosphate	1-Inositol Phosphate
Co-crystal/soak	-	co-crystal	30 min soak	8 h soak	5 days soak	co-crystal	brief soak
Beamline	MX2	MX1	MX1	MX1	MX1	MX2	MX1
Data collection							
Space group	$P2_12_12_1$	$P2_12_12_1$	$P2_12_12_1$	$P2_12_12_1$	$P2_12_12_1$	$P2_12_12_1$	$P2_12_12_1$
Unit cell dimensions	*a* = 59.01 *b* = 84.47 *c* = 98.37	*a* = 58.90 *b* = 84.50 *c* = 98.93	*a* = 59.58 *b* = 84.36 *c* = 98.96	*a* = 58.58 *b* = 84.43 *c* = 99.07	*a* = 58.66 *b* = 84.49 *c* = 98.99	*a* = 90.58 *b* = 98.80 *c* = 105.41	*a* = 59.12 *b* = 83.15 *c* = 99.39
Resolution (Å)	2.49 (2.58–2.49)	2.01(2.08–2.01)	2.42 (2.51–2.42)	2.21 (2.29–2.21)	1.99 (2.06–1.99)	2.30 (2.38–2.30)	2.50 (2.59–2.50)
Total reflections	117 013 (10 585)	244 996 (24 008)	141 608 (13 755)	184 421 (17 822)	251 425 (24 311)	1 020 200 (98 723)	238 389 (24 460)
Unique reflections	17 644 (1641)	33 688 (3255)	19 588 (1905)	25 322 (2472)	34 391 (3376)	42 818 (4426)	17 538 (1716)
Completeness (%)	99.4 (94.7)	99.8 (98.6)	99.7 (98.2)	99.9 (99.4)	99.8 (99.1)	100 (99.6)	99.9 (99.9)
R_{merge}	0.10 (0.76)	0.15 (0.70)	0.14 (0.66)	0.20 (0.86)	0.10 (0.39)	0.49 (1.44)	0.17 (1.43)
Average I/σ	13.2 (2.1)	12.6 (3.2)	13.5 (3.0)	10.1 (2.6)	17.7 (5.4)	5.9 (3.0)	14.4 (2.1)
Multiplicity	6.6 (6.5)	7.3 (7.3)	7.2 (7.2)	7.3 (7.2)	7.3 (7.2)	23.8 (22.3)	13.6 (14.3)
CC½	0.998 (0.849)	0.997 (0.824)	0.997 (0.928)	0.994 (0.782)	0.998 (0.948)	0.984 (0.925)	0.998 (0.765)
Refinement							
R_{work} (%)	18.5 (26.3)	15.6 (19.8)	18.1 (24.5)	17.8 (22.7)	16.1 (17.5)	17.3 (20.1)	17.2 (22.6)
R_{free} (%)	24.6 (32.0)	21.4 (31.2)	23.7 (31.8)	23.9 (30.2)	19.6 (24.7)	22.3 (25.9)	26.5 (33.7)
Protein atoms	3739	3818	3745	3751	3819	7352	3688
Ligand atoms	18	23	38	38	38	86	34
Water molecules	44	480	94	143	292	292	140
RMS (bonds) (Å)	0.007	0.007	0.007	0.007	0.007	0.008	0.008
RMS (angles) (°)	0.95	1.14	0.99	0.98	1.03	1.01	1.00
Ramachandran favoured (%)	93.6	96.2	95.0	95.6	96.4	96.0	94.5
Ramachandran outliers (%)	0	3.8	0.6	0.6	0	0.2	0.2
Average B-factors ($Å^2$)	50.6	21.9	35.5	26.9	20.9	21.3	45.0

Values in parentheses are for the highest resolution shell.

computed atlas of surface topography of proteins (CASTp) server [24] indicates a larger catalytic pocket volume (solvent accessible surface volume for the pocket is 224.4 $Å^3$ for the WT enzyme and 540.7 $Å^3$ for the TNYR variant).

The introduction of an amino acid with a side-chain, such as threonine, at position 186 changed the interaction network of this residue from that observed in the WT protein or a parent NYR mutant enzyme. T186 makes two hydrogen bond contacts to the side-chain of S87 (side-chain to side-chain and main-chain to side-chain) and main-chain of N93 (main-chain to main-chain), in addition to four van der Waals interactions with M72, S87, P92 and F96 (Supplementary Figure S3A). In the WT SaPLD, a hydrogen bond contact is seen between G186 and N93, while a water molecule bridges the hydrogen bonding interactions between G186 and S87 (PDB: 2ZE4, Supplementary Figure S3B). For the WT PLD, the hydrophobic network includes P92, F96, N185 and W187. An extra hydrogen bond combined with the van der Waals interaction network directed

Biochemical Journal (2021) **478** 1749–1767
https://doi.org/10.1042/BCJ20210117

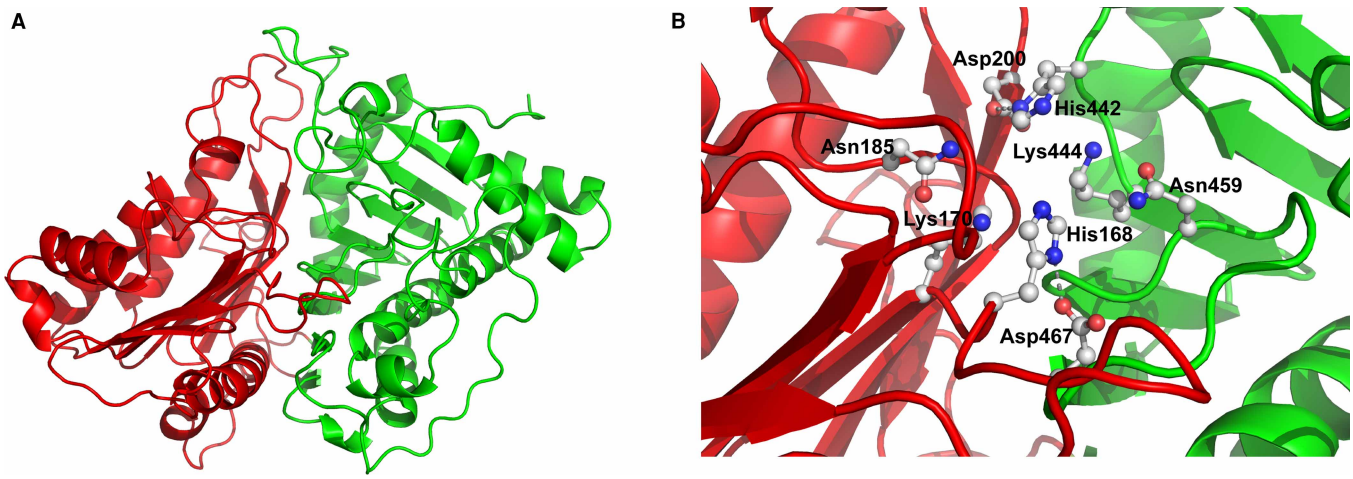

Figure 1. Structure of the TNYR mutant of SaPLD.

(**A**) Secondary structure representation showing the pseudo-dimeric architecture. The N-terminal lobe is coloured red and the C-terminal lobe coloured green. (**B**) The active site region of the structure with key catalytic residues on each lobe shown in ball and stick representation.

towards the residues of the inner cavity rather than the substrate-binding site in TNYR SaPLD seems to hold the loop containing the residues 182–188 in a shape conducive to accommodate *myo*-inositol in an orientation suitable for 1-PI synthesis.

The arginine mutation at position 385 lies on one of the surface loops (377–385) proposed to make up the substrate entry point. The loop appears to be very flexible, which is evident by the weaker electron density in this region of the map. We have modelled the loop at a lower contour level (1.00 σ). A polder OMIT map [25] contoured at 3.00 σ has confirmed that the first and the last residue of the loop have been correctly modelled

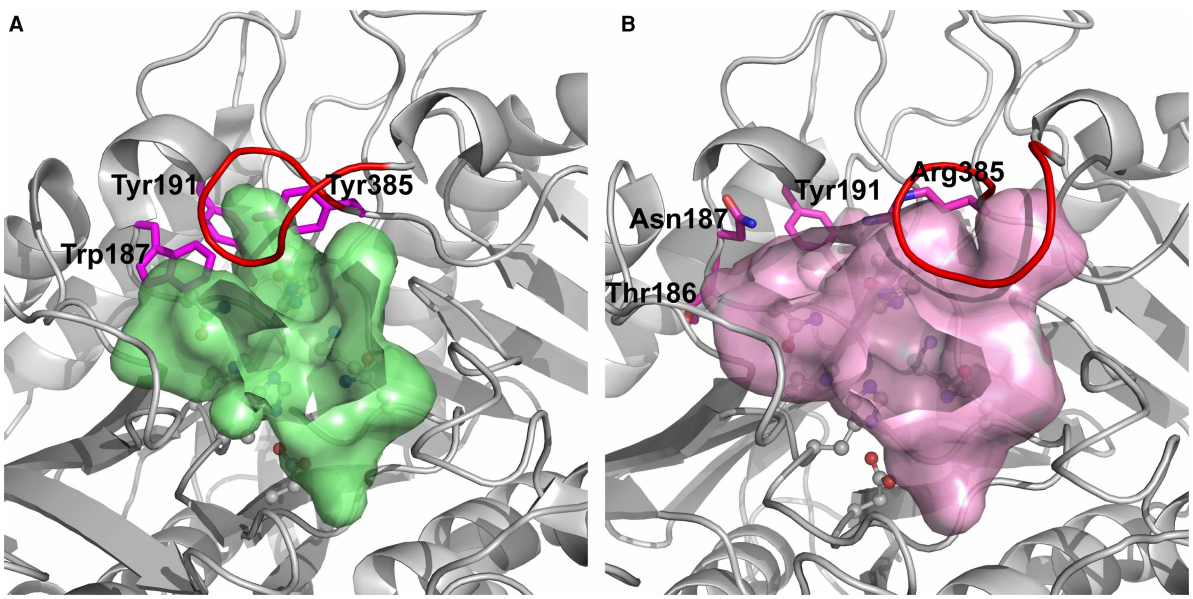

Figure 2. The structural consequences of the TNYR mutations to SaPLD.

(**A**) The secondary structure of the WT SaPLD (PDB: 2ZE4) showing the substrate binding pocket as a green coloured surface. (**B**) The secondary structure of the TNYR variant of SaPLD showing the substrate-binding pocket as a pink coloured surface. The residues that have been mutated are shown in magenta coloured sticks. The key catalytic residues on each lobe are shown in ball-and-stick representation. Residues 378–384 on the substrate entry loops are coloured red. The pocket volume for each of the structures has been computed with the CASTp server [5].

Biochemical Journal (2021) **478** 1749–1767
https://doi.org/10.1042/BCJ20210117

(Supplementary Figure S4A). This arginine side-chain lies in a similar position to the tyrosine residue in the WT enzyme and both the arginine and the tyrosine side-chains make hydrogen bond contacts to the carboxylate group of D190 (Figure 3A,B). However, the presence of an asparagine side-chain at position 187 in the mutant structure, rather than a tryptophan, causes a reorientation of the side-chain of D190 relative to the WT structure resulting in the formation of an additional hydrogen bond interaction. The positively charged arginine side-chain and the polar asparagine side-chain are likely to alter the electrostatic nature of the larger pocket to better accommodate the bulkier polar *myo*-inositol ligand.

A comparison between the TNYR structure and the WT enzyme structure was made for the surface loop consisting of residues 377–385, proposed to be involved in substrate entry into the active site. Modelling of the substrate entry loop in the mutant shows that it adopts a different conformation than that observed in the WT structure and this reorientation of the loop appears to contribute to the large catalytic pocket volume described above (Figure 2A,B and Figure 4). The loop in the WT structure appears more closed with the tip of the loop lying close to the side-chain of W187 (van der Waals interaction between the indole ring of the tryptophan residue and the main-chain of the loop particularly in the region of G381). In contrast, in the TNYR mutant the loop is drawn back to generate a larger binding pocket and there are no van der Waals interactions between N187 and G381.

Thus, the overall effects of the different side-chain orientations and contacts that occur through the mutations, resulting in a larger binding pocket to encompass a larger substrate, conformational changes of the loops involved in substrate entry and substrate recognition and the orientation of the loops may all contribute to altering substrate access and substrate binding specificity in the TNYR mutant.

Structure of TNYR SaPLD in complex with phosphate

Initial attempts to obtain a complex structure of the TNYR mutant with *myo*-inositol were unsuccessful as electron density maps obtained from crystals soaked in the presence of the ligand failed to show significant interpretable density for the ligand. Further attempts to obtain a structure of the TNYR mutant with *myo*-inositol were carried out by co-crystallising the enzyme in the presence of 20 mM KH_2PO_4 and 20 mM *myo*-inositol. It was thought that the bound phosphate ion would mimic an enzyme intermediate state thus enabling better recognition and binding of the *myo*-inositol substrate without allowing the enzyme to do the turnover. Data were

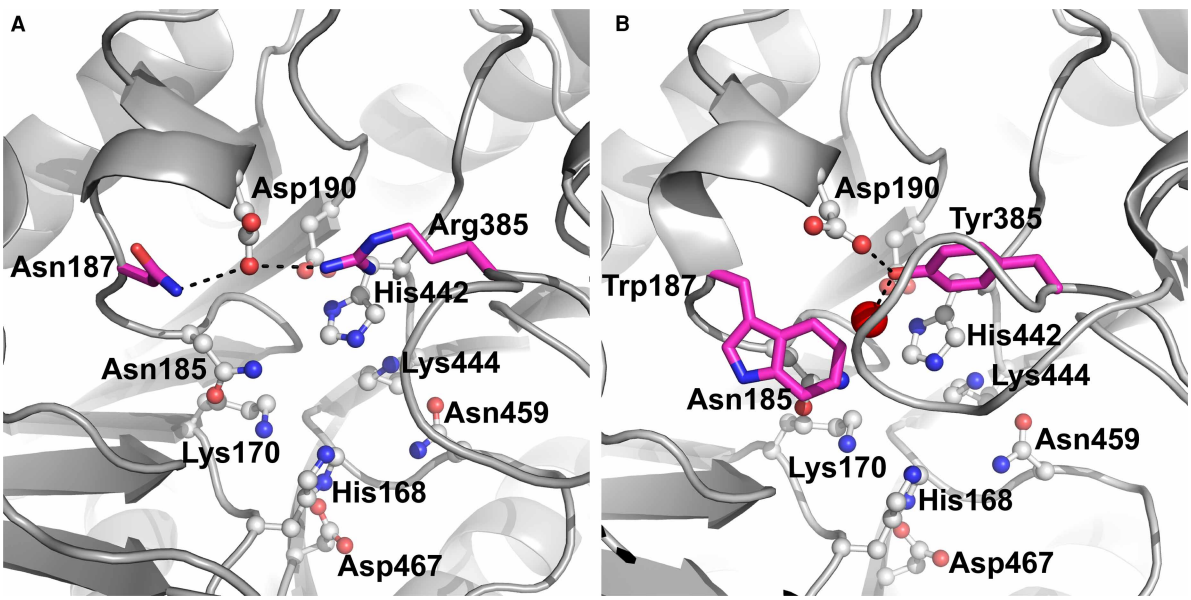

Figure 3. Comparison of contacts and substrate access loop conformation for WT SaPLD and the TNYR variant.
(**A**) Contacts in the active site region for the TNYR variant. (**B**) Contacts in the active site region for the WT SaPLD structure. The WT residues and their mutations in the TNYR structure are shown in magenta coloured sticks. The key catalytic residues on each lobe are shown in ball-and-stick representation. The water molecule is shown as a red sphere. Hydrogen bonds are shown in black dashed lines.

Biochemical Journal (2021) 478 1749–1767
https://doi.org/10.1042/BCJ20210117

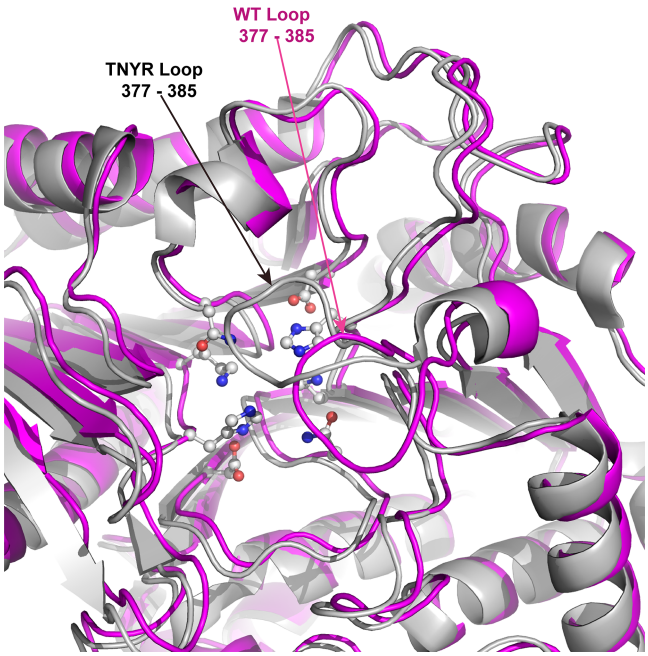

Figure 4. Superposition of structures of the TNYR mutant and WT SaPLD.

The TNYR mutant structure is coloured in magenta and the WT structure is coloured grey. The side-chains for the key catalytic residues of the TNYR structure are shown in ball-and-stick representation. The surface loops consisting of residues 377–385 are indicated by arrows for each structure.

collected to 2 Å resolution and processed (see Table 1), and the structure solved by molecular replacement as described above. The electron density map revealed positive difference density into which a phosphate ion could be modelled and refined (Figure 5A). However, no difference density was apparent into which the *myo*-inositol could be included in the model.

The phosphate ion makes hydrogen bond contacts with the side-chains of H168, H442, Q337, Y461, K444, N459, R385 and a catalytic water molecule, which in turn makes hydrogen bond interactions with the side-chains of K170 and N185. This finding aligns well with the previous reports about conserved lysine and asparagine residues of the active site having the stabilising effect on the enzyme-substrate intermediate by binding and neutralising the phosphorous [22,26]. The loop from residues 377–385 adopts a different orientation and the side-chain for R385 shifts significantly and makes a weak hydrogen bond contact with one of the oxygen atoms of the bound phosphate ion (Figure 6B). The reorientation of this loop further seals off the substrate-binding site relative to the structures of the empty TNYR mutant, and the empty WT enzyme. Despite this reorientation, the electron density around the loop is stronger compared with the empty structure which enables confident modelling of the loop. Correct modelling of the loop has been confirmed by a polder OMIT map contoured at 3.00 σ that encompassed the entire loop (Supplementary Figure S4B). Additionally, although the loop lies close to the crystal packing interface, intermolecular contact analysis confirmed that the loop does not make contacts with the neighbouring molecules, and therefore we conclude that the movement of the loop appear to be solely due to the binding of the phosphate ion.

The hydrogen bonds and van der Waals interactions of T186 are also seen in this structure and resemble those observed in the empty TNYR structure. In this case, a water molecule that forms hydrogen bonds to the side-chain of S87 and the main-chain of T186 is added to the hydrogen bond network of T186, while the van der Waals interaction with S87 is notably absent from this structure.

Structures of TNYR SaPLD in complex with PA

To further probe substrate binding, crystals of the TNYR mutant were soaked in mother liquor solutions containing 2 mM 1,2-dibutyryl-*sn*-glycero-3-phosphocholine (diC_4PC), the enzyme's substrate, for different time

Biochemical Journal (2021) **478** 1749–1767
https://doi.org/10.1042/BCJ20210117

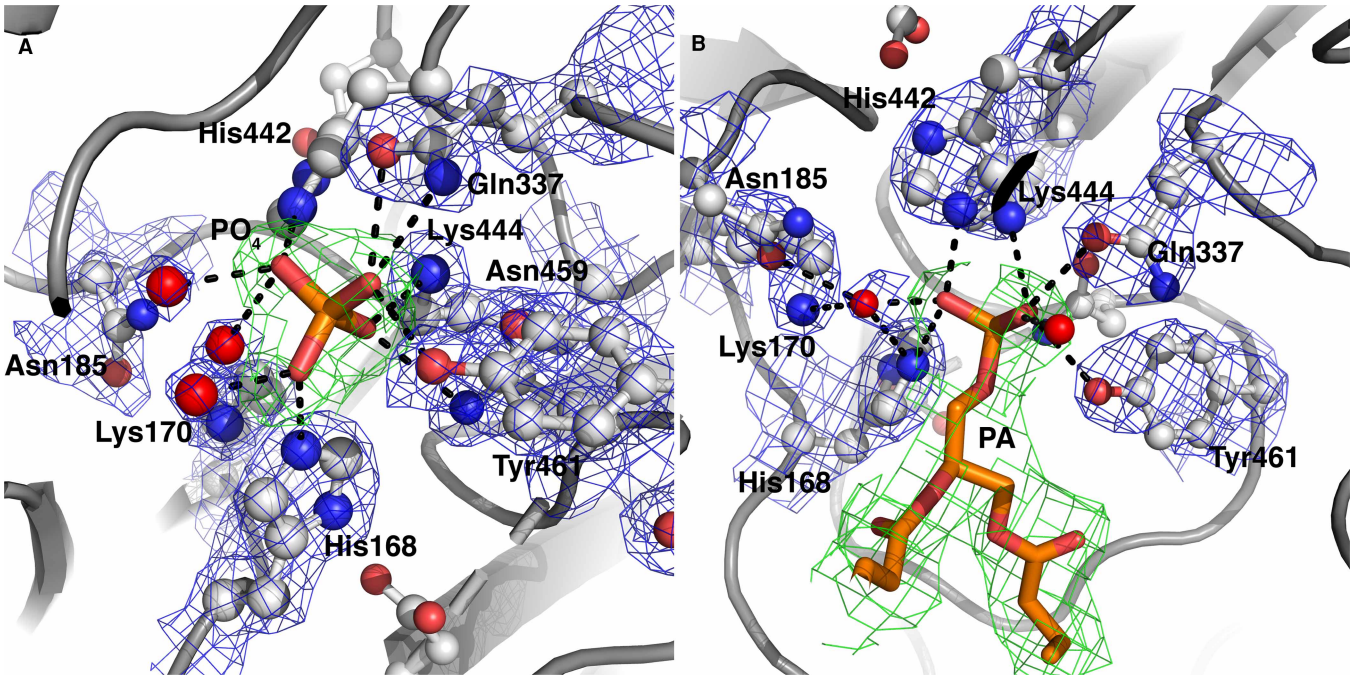

Figure 5. Electron density maps for bound ligands in the TNYR SaPLD structure.

(**A**) 2Fo-Fc electron density map of the phosphate bound TNYR structure and the polder OMIT map for the phosphate. (**B**) 2Fo-Fc electron density map of the PA bound TNYR structure (soaked for 30 min) and the polder OMIT map for the bound PA. The 2Fo-Fc electron density maps are shown in blue and are contoured at 1.2 σ. The polder OMIT maps are shown in green and are contoured at 3 σ. Phosphate (PO_4^{3-}) and PA are shown as orange sticks. Protein side-chains are shown in ball-and-stick representation. Water molecules are shown as red spheres. Hydrogen bonds are shown in black dashed lines.

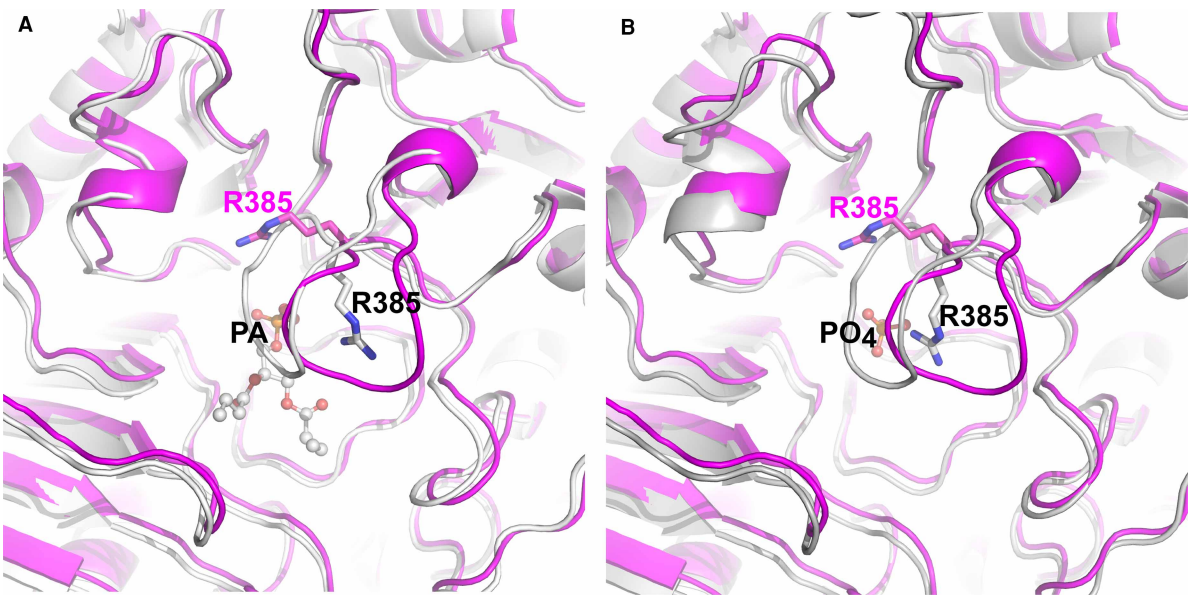

Figure 6. Comparisons of ligand bound and empty TNYR SaPLD structures.

(**A**) Superposition of the unliganded TNYR mutant and the PA bound TNYR mutant (30 min soak). (**B**) Superposition of the unliganded TNYR mutant and the phosphate (PO_4^{3-}) bound TNYR mutant. The unliganded structure is in magenta and the ligand bound structures are in light grey. PA and PO_4^{3-} are shown in ball-and-stick representation. R385 for the two structures are shown in white bonds and magenta bonds matching the ribbon diagram colours.

Biochemical Journal (2021) **478** 1749–1767
https://doi.org/10.1042/BCJ20210117

periods (30 min, 8 h and 5 days). The data collection and refinement statistics are shown in Table 1. The electron density maps from all three data sets revealed only features of the PA suggesting that the choline moiety has been cleaved by the action of H168 and H442 after the formation of the phosphatidyl intermediate, leaving the PA bound and choline released from the enzyme. The density for the PA ligand was the weakest for the 5 day soaked crystals and strongest for the 30 min soaked crystals (Figure 5B). This is despite the fact that resolution was highest and the refinement statistics were the best for the 5 day soaked crystals (see Table 1). This indicates that the PA ligand may have been released from the binding site after a longer period of time. In all three structures, density for a water molecule is observed midway between one of the phosphate oxygen atoms of PA and the side-chain of N185. In the 5 day soaked structure this side-chain adopts two positions, one (60% occupancy) in hydrogen bond contact to the water molecule and one (40% occupancy) where the side-chain is turned away from the water and makes hydrogen bond contact with the main-chain nitrogen of L88.

Comparisons of the three PA bound structures with the unliganded structure and the phosphate bound structure revealed differences in the orientation of the substrate entry loop (377–385). This loop adopts a similar conformation in both the PA and the phosphate bound structures, closing the substrate-binding site from the external enzyme environment. In contrast, in the unliganded TNYR structure, this loop adopts a more open conformation exposing the substrate-binding site to the exterior environment of the protein (Figure 6A,B). This change in the loop position also alters the orientation of R385 in the structures; in the ligand-bound structures, the arginine side-chain is directed inwards towards the ligand while in the unliganded structure the arginine side-chain is more surface exposed.

Interestingly, in the unliganded WT enzyme (PDB: 2ZE4), loop 377–385 adopts a closed conformation, similar to both the phosphate and PA bound TNYR structures. In contrast, the loop in the H168A mutant — PA bound structure (PDB: 2ZE9), adopts an open conformation. The position of Y385 in 2ZE4 and 2ZE9 structures coincides with the position of R385 in the unliganded TNYR structure in contrast with the inward-directed arginine side-chain in the ligand-bound structures (Figure 7).

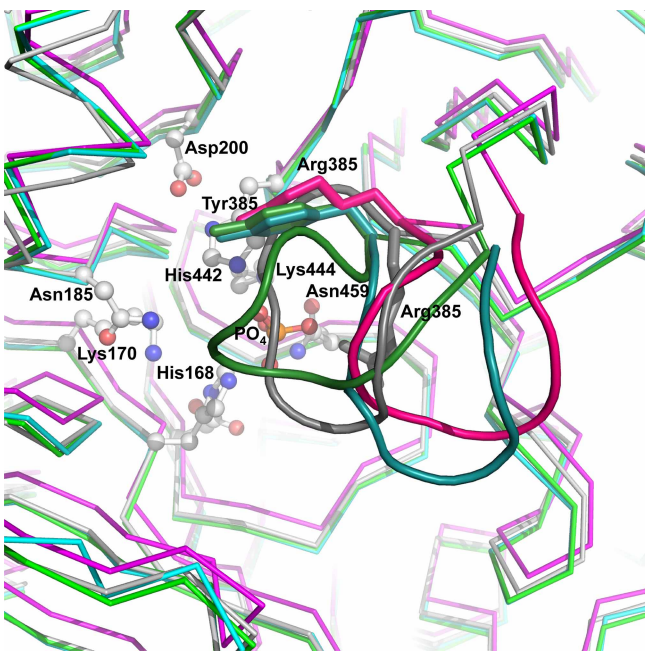

Figure 7. Overlay showing the loop conformations in four different structures.
The unliganded TNYR structure is coloured magenta, in teal is the structure of the H168A mutant bound to PA (PDB: 2ZE9), in green is the WT unliganded structure (PDB: 2ZE4) and in grey is the TNYR structure bound to phosphate. The side-chains for the key catalytic residues are shown in ball-and-stick representation and correspond to the positions of these residues in the phosphate bound TNYR structure. The phosphate is in ball-and-stick representation with orange bonds. The side-chains of residue 385 are shown in the colour corresponding to that of the ribbon/cartoon representation. The substrate entry loop (residues 377–385) for each structure is shown in coil representation and coloured as detailed above.

Biochemical Journal (2021) **478** 1749–1767
https://doi.org/10.1042/BCJ20210117

A detailed comparison of the position of the bound PA in the TNYR structure and the H168A mutant enzyme reveals a shift of the phosphorous atom by 2.5 Å towards the expected location of the imidazole ring in the mutant enzyme (Figure 8). This shift is likely due to the mutation of the catalytic histidine 168 and the ligand position may mimic a covalent intermediate state. A superposition of the two PA bound structures shows that the phosphorous atom in 2ZE9 lies 1.3 Å and 4.2 Å from NE2 of H168 and NE2 of H442, respectively, while it is equidistant at 3.5 Å and 3.3 Å from the NE2 atoms of H168 and H442, respectively, in the TNYR structure.

In the case of the TNYR–PA complex structures, the hydrogen bond contacts to the phosphate moiety include H168, K170, Q337, H442, N459 and Y461 (Figure 5B). The shift in the position of the phosphate group between 2ZE9 and TNYR–PA complex structures removes a hydrogen bond interaction with N185 and adds interactions with Q337 and Y461. The interaction with Q337 links the phosphate group to the 377–385 loop through a hydrogen bond to the main-chain nitrogen of G384. Q337 does not make interactions with the loop in the 2ZE9 structure. This observation suggests that Q337 to G384 interaction may assist in closing the loop over the substrate-binding site contributing to the alternate conformation of this loop relative to the ligand-bound H168A mutant structure and the empty TNYR structure. Thus, the TNYR–PA complex structures may be interpreted as representing the enzyme-product bound states after cleavage and release of choline and after hydrolysis of the covalent H168-phosphatidyl intermediate. In contrast, the H168A–PA complex structure (2ZE9) may mimic a covalent bound intermediate state (albeit without the covalent linkage due to the absence of the side-chain for H168).

As for the T186 residue, it was found to form an interaction network identical with that seen in the structure of the TNYR-phosphate complex. The hydrogen bond network of T186 includes S87, N93 and a water molecule that mediates hydrogen bonding with S87. The water molecule is only absent from the 30 min-soaked structure. The interaction between the side-chains of S87 and T186 is considerably weaker in the 30 -min-soaked structure (3.6 Å) and in the 5 day-soaked structure (3.31 Å and 3.5 Å; the 5 day-soaked structure shows S87 in two conformations). Van der Waals interactions are formed with residues M72, S87, P92 and F96 regardless of soaking time.

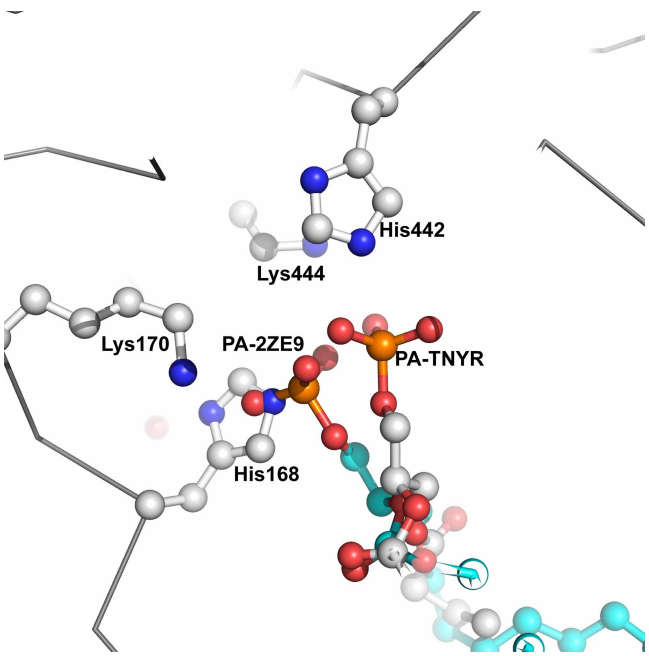

Figure 8. Comparison of the position of PA in the TNYR mutant structure and in the H168A mutant structure (PDB: 2ZE9).

The PA is shown in white ball-and-stick representation for the TNYR structure and in teal ball-and-stick representation for the H168A mutant structure. The side-chains of key active site residues are shown for the TNYR structure bound to PA.

PORTLAND PRESS

Biochemical Journal (2021) **478** 1749–1767
https://doi.org/10.1042/BCJ20210117

Structures of TNYR SaPLD in complex with 1-inositol phosphate

In a further attempt to visualise the presence of *myo*-inositol in the TNYR structure, crystals were soaked with the product analogue, 1-inositol phosphate (prepared as described in the Materials and Methods section). However, the electron density maps from these crystals failed to show density for the *myo*-inositol moiety. Following this, a co-crystallization approach was undertaken. Crystals of the TNYR SaPLD were grown in the presence of the ligand and harvested after 28 days. Three datasets were collected from two different crystals. The datasets were merged and used to solve the structure to 2.3 Å resolution (Table 1). Interestingly the crystals were indexed on a different lattice with two molecules in the asymmetric unit. The electron density clearly indicated the presence of the ligand covalently linked to H442. A model for a covalently modified histidine consisting of 1-inositol phosphate linked to the NE2 atoms of the imidazole ring of histidine was incorporated into the structure and refined. The tetrahedral phosphate group linked to the histidine side-chain has the strongest electron density. The density becomes significantly weaker for the inositol moiety of the ligand and the high temperature factors suggest that the ring is highly mobile (Figure 9A). A polder OMIT map contoured at 3.0 σ verified the presence of the modelled inositol moiety (Figure 9B). As expected, the absence of the tryptophan side-chain at position 187 provides space for the inositol ring to bind to the enzyme thus increasing the size of the binding pocket to accommodate a larger substituent. The loop from residues 377 to 386 is not visible in

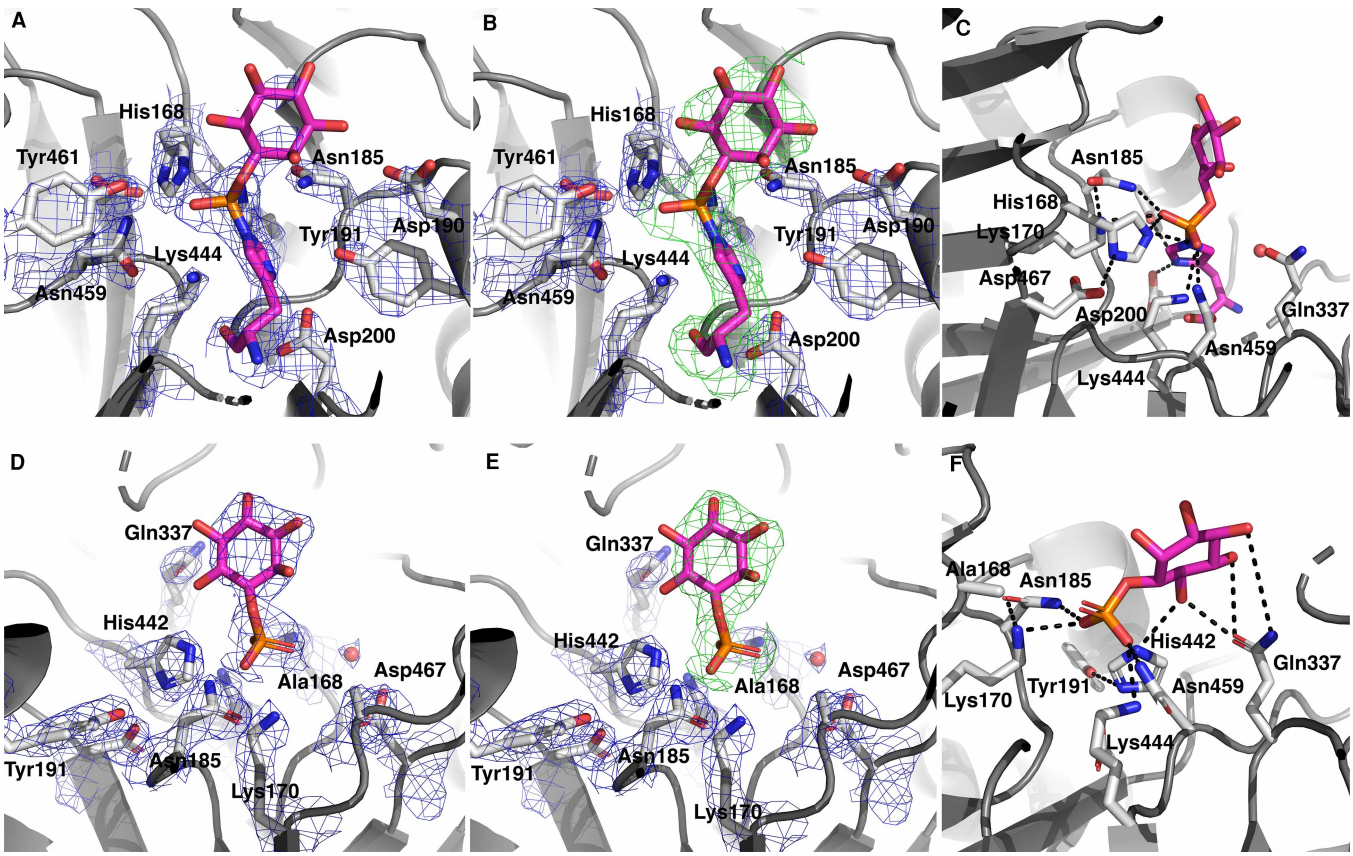

Figure 9. The structure of the TNYR mutant complexed to 1-inositol phosphate.

(**A**) 2Fo-Fc electron density map of the active TNYR mutant showing 1-inositol phosphate covalently linked to His442. (**B**) 2Fo-Fc electron density map of the active TNYR and the polder OMIT map for the covalent adduct. (**C**) Hydrogen bond contacts between the protein and the covalently bound ligand. (**D**) 2Fo-Fc electron density map of the inactive (H168A) TNYR mutant showing 1-inositol phosphate non-covalently bound. (**E**) 2Fo-Fc electron density map of the inactive (H168A) TNYR mutant and the polder OMIT map for the 1-inositol phosphate. (**F**) Hydrogen bond contacts between the protein and the non-covalently bound ligand. The 2Fo-Fc electron density maps are shown in blue and are contoured at 1.0 σ. The polder OMIT maps are shown in green and are contoured at 3.0 σ. The ligand, including the covalently linked His442, is shown in magenta coloured sticks. Hydrogen bond contacts are shown in black dashed lines.

Biochemical Journal (2021) **478** 1749–1767
https://doi.org/10.1042/BCJ20210117

either of the molecules in the asymmetric unit. The phosphate oxygen atoms lie within hydrogen bond contact from NE2 of H168 (Figure 9C). The enzymatic reaction that results in the formation of the covalent intermediate requires a protonation of the hydroxyl group on the phosphate to make a leaving group followed by a nucleophilic attack on the phosphorous atom with the release of water. The close proximity of H168 to the oxygens and the orientation of this side-chain suggest that it may act as the acid for the protonation of the phosphate hydroxyl group.

To test the role of H168 in the formation of the covalent adduct to H442, the crystal structure was also determined for the inactive TNYR mutant where H168 had been mutated to alanine (H168A TNYR). In this case, the crystals were soaked briefly in a cryo-protectant that contained 1-inositol phosphate. The brief soak method was carried out to minimise the damage to the crystals since they tended to crack upon soaking in artificial mother liquor containing the ligand. The structure was determined at 2.5 Å resolution (Table 1). In this structure the electron density revealed 1-inositol phosphate bound in the structure with the phosphate moiety not covalently linked to H442 (Figure 9D). The density for the phosphate moiety of the ligand was well delineated, while the density for the inositol portion was weaker but still evident in the polder OMIT map (Figure 9D,E) suggesting more flexibility in this portion of the ligand. The structure does however show differences in the position of the inositol moiety between the two structures (Figure 9C,F and Figure 10). Additionally, the position of the phosphorous atom differs in the two structures by 1.7 Å (Figure 10).

The observation of electron density in the crystal structure of the active TNYR enzyme clearly showing the covalent linkage between the ligand and H442 rather than H168 and the absence of this linkage in the structure of the H168A mutant enzyme suggests that H168 may act as an acid in protonation of the phosphate hydroxyl group resulting in a better leaving group (H_2O) after nucleophilic attack from H442 at the phosphorous atom to form the covalent linked intermediate (see the proposed mechanism in Figure 11).

Discussion

PLD-catalysed transphosphatidylation of a phosphatidyl group from one alcohol acceptor to another results in a novel PL with a different head group. It is especially important for the synthesis of unnatural or low-abundance PLs. Previously, SaPLD was engineered to broaden the enzyme's substrate specificity and overcome its limitation regarding the size and shape of the acceptor compounds [10]. Through three rounds of site-

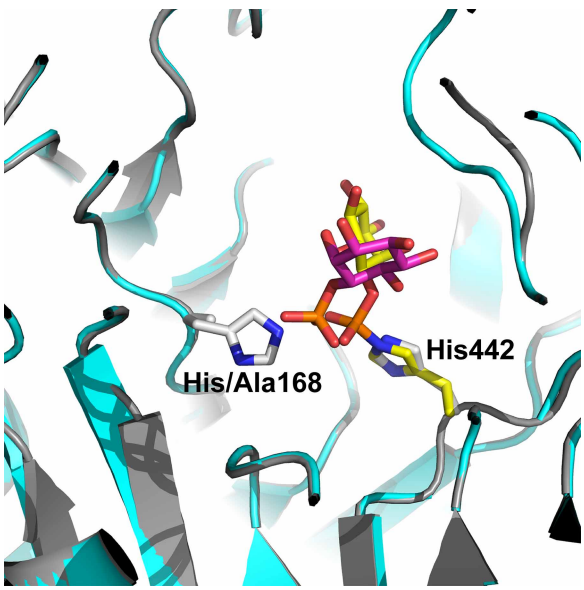

Figure 10. Comparison of the 1-inositol phosphate positions.

Superposition of the structures of the active TNYR mutant containing the covalent linkage between 1-inositol phosphate and His442 and the inactive TNYR mutant (His168A) containing the 1-inositol phosphate non-covalently bound to the enzyme. The ribbon representation for the active mutant structure is coloured grey and that for the inactive mutant is coloured cyan. The covalently bound ligand is shown in yellow coloured sticks and the non-covalently bound ligand is shown in magenta coloured sticks.

Biochemical Journal (2021) **478** 1749–1767
https://doi.org/10.1042/BCJ20210117

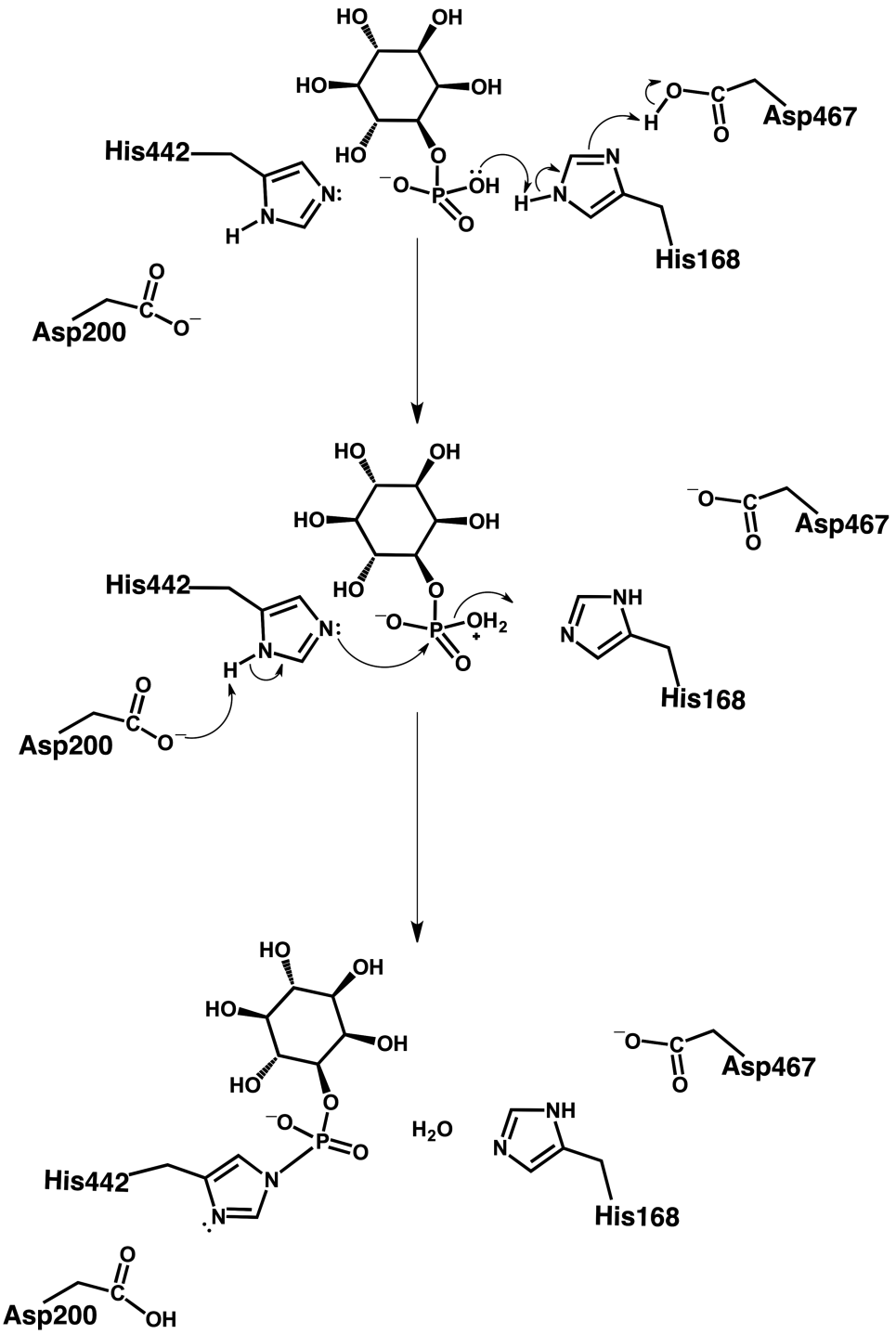

Figure 11. TNYR SaPLD mechanism.

Proposed mechanism for the formation of the 1-inositol phosphate-TNYR SaPLD intermediate.

directed saturation mutagenesis, a mutant, namely TNYR SaPLD (G186T, W187N, Y191Y, Y385R) was obtained. The mutant is capable of producing 1-PI, the only natural PI isomer, with positional specificity of up to 98% [12].

Crystallographic studies of the mutant protein have been carried out to better understand the molecular details for substrate binding and the mechanism that enables the synthesis of 1-PI. Analysis of the mutant structure and

comparisons with the WT enzyme show that the mutations have provided a larger catalytic pocket volume and wider opening area to accommodate binding of a bulky *myo*-inositol as an acceptor of the phosphatidyl moiety. Additionally the introduction of more polar residues, are more favourable for hydrogen bonding with the substrate, and might contribute to the broadened substrate specificity of the enzyme. Residue 191 is thought to be in contact with the polar head of PLs and important for stabilising the quaternary ammonium group of choline by the formation of a cation-π interaction. In fact, a large number of 1-PI synthesising SaPLD mutants with high positional specificity retained Tyr at position 191 [10,11], thus it is likely that this residue also interacts and stabilises the inositol ring. In our work, Y191 forms a hydrogen bond with the main-chain nitrogen of N185 in almost all TNYR structures. Interestingly, this hydrogen bond is also present in WT SaPLD structures, 2ZE4 and 2ZE9. Based on this observation, Y191 could also be involved in maintaining the shape of the acceptor-binding loop. While residue 385 shows a very interesting behaviour its role in PI-synthetic activity is yet to be fully explained. The arginine side-chain is positioned quite differently from the tyrosine side-chain in the WT enzyme. The side chain of R385 rotates dramatically toward the bound phosphate ligand, a movement not observed in the WT structure. In fact, the entire 377–385 loop moves in a different manner than in the WT SaPLD enzyme and this shift is accompanied by a change to the position of residue 385.

In addition to the PLD structures from *S. antibioticus* discussed above, a structure of a homologues PLD from *Streptomyces sp.* strain PMF has been solved [22]. This work reports a number of structures including a series of complexes of the enzyme with the substrate diC_4PC obtained with different soak times as was carried out in our work. Interestingly, in these structures, a covalent adduct between the active histidine (H170) and the phosphate group of the PA product was able to be visualised in the electron density maps at 30 min soak time and a water molecule had attacked this covalent adduct to generate a pentacoordinate phosphate (PDB: 1V0Y). In addition, after longer soak times (8 h and 8 days) a phosphate was seen covalently bound to H170 and the side-chain was also observed in multiple conformations. Notably, in all of these structures, the loop coinciding with residues 377–385 in the SaPLD has no density and has therefore not been included in the models. The lack of electron density can be caused by a disordered conformation of the loop often due to the flexible nature of specific residues and/or residues that are largely exposed to the solvent [27] and is indicated by high B-factor values [28]. The unliganded TNYR structure exhibits a high overall B-factor value (mean isotropic B-factor = 50.66 $Å^2$) compared with the unliganded WT SaPLD (mean isotropic B-factor = 21.58 $Å^2$), however, the normalised B-factors of the loop of the two structures are similar (Supplementary Table S1 and Supplementary Figure S5). Interestingly, the electron density of the loop in the unliganded TNYR is not as strong as that of the unliganded WT SaPLD. In contrast, the overall B-factor of the TNYR–PA complex soaked for 30 min (where the electron density of the loop is the strongest among the PA soaked TNYR structures) is higher (35.6 $Å^2$) compared with the WT SaPLD–PA complex structure (16.0 $Å^2$), while the normalised B-factor of the WT SaPLD–PA complex structure is much higher (Supplementary Figure S5) which corresponds to the weaker electron density. The 377–385 loop shows weak electron density when it adopts an open conformation, such as in the unliganded TNYR and the WT SaPLD–PA complex structure. When the loop adopts a closed conformation, it becomes less exposed to the solvent, resulting in stronger electron density.

Additionally, in the TNYR structure with the covalent adduct of 1-inositol phosphate on H442 and in the inactive TNYR structure complexed with 1-inositol phosphate, the 377–385 loop cannot be modelled due to a lack of electron density. In the two structures of TNYR in complex with 1-inositol phosphate, the bound ligand appears to act as a substrate rather than a product analogue. Superposition of the inactive TNYR with PMF PLD (PDB: 1V0Y) suggests that the 1-inositol phosphate in the inactive TNYR structure is oriented towards the bound ligand in the PMF PLD structure. In the covalently bound 1-inositol phosphate structure, the inositol moiety also lies in a similar orientation to the fatty-acyl chain of the PA in the PMF PLD structure suggesting that the enzyme recognises 1-inositol phosphate as a substrate (Supplementary Figure S6). Therefore, it is likely for the TNYR variant, that the flexible loop adopts an open conformation when the protein is unbound or bound to the substrate. The loop reorients itself to adopt a closed conformation for catalysis and, after the reaction has occurred and the products have been released, the loop reorients back to an open conformation. Based on this interpretation, we suggest that substrate binding in the TNYR SaPLD occurs in a different manner compared with that of the WT SaPLD, and that the observed structural rearrangement likely contributes to the larger volume of the active site.

Previously, screening of G186X NYR variants with improved 1-PI positional specificity yielded the best performing variant, TNYR [12]. Besides TNYR, four other 186X mutants with highly improved 1-PI specificity (>91%) included L186, V186, S186 and M186. Based on the work of Negishi et al. [29], who reported that

Biochemical Journal (2021) 478 1749–1767
https://doi.org/10.1042/BCJ20210117

G188 in *Streptomyces septatus* TH-2 PLD (TH-2PLD), which corresponds to the G186 in WT SaPLD, plays a crucial role in the thermostability of this enzyme, we hypothesised that mutating glycine to other residues may change the local structure's dynamics to enable better binding of *myo*-inositol in the orientation leading to the synthesis of 1-PI. To test the hypothesis, we used TNYR, L186 NYR (LNYR) and NYR for PI synthesis at a temperature range from 10 to 37°C. As expected, at low temperatures 1-PI positional specificity was improved in all three enzymes, with TNYR and LNYR showing better performance than NYR. While TNYR synthesised 1-PI with positional specificity of 93% at 37°C, it was further improved to 98% at 10°C. At lower temperatures the protein structure is likely to be less mobile, and our result suggests that this lower mobility is better for 1-PI specificity. Results from this work suggest that local changes in protein dynamics could be the result of the additional hydrogen bond contact between S87 and T186, however LNYR, V186 NYR and M186 NYR cannot form such hydrogen bonds. However, the hydrophobic interaction network differs significantly among G186 and other bulkier residues, such as Thr, Val, or Leu. In structures of TNYR, the hydrophobic interaction network of T186 is formed with the residues of the inner cavity behind the substrate-binding loop, unlike the network of G186 in WT SaPLD, and we believe that this, in addition to an extra hydrogen bond with S87 observed in TNYR, contributes to a change in loop (182–188) dynamics that facilitates binding of *myo*-inositol in an orientation favoured for 1-PI synthesis.

While complex structures in the presence of *myo*-inositol could not be determined, we were able to characterise structures in the presence of phosphate, diC_4PC and 1-inositol phosphate, which allowed visualization of the bound ligands. The binding of the phosphate ion and the phosphate group of PC occurs at the same position relative to the catalytic histidines.

The choline portion of the PC was not observed suggesting that it has been cleaved during the soaking, resulting in structures with bound PA. Comparison of the TNYR structure in complex with PA and WT SaPLD (2ZE9) reveals the difference in positioning of the phosphate group of 2.5 Å, which may suggest that we are visualising the ligand position at different stages of the catalytic cycle. The phosphate group position in the 2ZE9 structure aligns well with that of the 1V0Y (PMF PLD covalent adduct with PA), and this is the actual position of the phosphate in the enzyme-substrate intermediate. As the intermediate is resolved, the phosphate group moves away from H168 to lie equidistant from the two histidine side-chains.

The PA-bound structures obtained after different soaking times indicate that the catalysis proceeded too fast for the substrate or intermediate to be captured. Because the catalysis proceeds in the crystal state, diffusion of PA from the binding site may have been hampered and its electron density could have been observed even after a 5-day long soak. The fact that the PA density is strongest in the 30 min soak and weakest in the 5-day soak indicates that to some degree, PA is still able to leave the binding site. The appearance of the alternative N185 conformation in some of the complex structures could indicate the role of this residue in the product release. In the structures representing the intermediate state (1V0Y and 2ZE9), N185 hydrogen bonds to the phosphate moiety supporting its role in phosphate coordination. However, in the phosphate and PA bound structures, N185 no longer coordinates the phosphate and, in phosphate and PA bound (5-day soak) structures the side chain shifts away from the product, as if it allows for the product release.

The greatest surprise came with the structure of the TNYR SaPLD co-crystalised with 1-inositol phosphate. Here we observed extra electron density attached to the side-chain of H442 corresponding to the phosphate group. This is the first structural evidence that the catalytic histidine residue in the C-terminal lobe of PLD can form the covalent adduct with phosphate. For this to occur, we hypothesise that the H168 needs to assume the role of acid and protonate the phosphate (Figure 11). This would produce water as a leaving group, leaving the phosphate susceptible to nucleophilic attack by H442, and subsequent formation of the covalent adduct. Once this adduct is formed, it could either stay unchanged or undergo a nucleophilic attack by the water molecule activated by H168 acting as a base. This would result in hydrolysis of the phosphoester bond between the phosphate and inositol, leaving the phosphate group bound to H442. Currently, we cannot say with high certainty whether the hydrolysis stops after the release of water or after the release of *myo*-inositol, since the electron density for the inositol ring is not very strong. We have interpreted this as a high degree of inositol ring mobility but it may also include partial hydrolysis of the phosphoester bond. Leiros et al. [22] have also suggested that the hydrolysis of the second phosphoester bond of PC in the crystal state of PMF PLD occurs, and the likelihood of a similar event in TNYR SaPLD cannot be fully excluded.

Formation of the covalent adduct with a C-terminal histidine may seem unusual, however, several previous reports have described similar phenomena in PLD and PLD superfamily members. Before the report on the catalytic mechanism of PMF PLD, our group published quite a different finding based on the biochemical experiments

conducted with the WT SaPLD [30]. Based on the bilobed structure of SaPLD, its sequence was divided into half, with each, N- and C-terminal lobe, expressed separately in recombinant *E. coli* as an inclusion body. The insoluble N- and C-lobe proteins were solubilised with a denaturant, mixed and refolded by removing the denaturant to reconstitute an enzymatically active, hetero-dimeric SaPLD. The hetero-dimeric SaPLD was treated with its substrate, fluorescently-labelled phosphatidylcholine, and analysed by denaturing SDS–PAGE. Since the positions of the N- and C-lobe proteins can be distinguished on the gel, UV irradiation allowed us to determine which band was fluorescently labelled; that is, which His residue (H168 or H442) acted as the nucleophile. As the result, the C-lobe was fluorescently labelled. Based on this observation, we concluded that H442 plays the role of the nucleophile and H168 plays the role of the general acid/general base (GA/GB). However, since this conclusion was soon rebutted, we paused further research about it until now, when we obtained new evidence, which indicates a certain plasticity of the substrate activation and catalysis. Although our present experiments utilised a product analogue, 1-inositol phosphate, and a mutant SaPLD, it undoubtedly demonstrates that the roles of the nucleophile and the GA/GB chemistry can be performed by either of the histidine side-chains under the right circumstances. We are currently conducting more studies with the WT SaPLD to further verify this new concept.

If we look at the other PLD superfamily members, such as endonuclease Nuc, which is a homodimeric enzyme utilising the same catalytic mechanism, the possibility of role exchange becomes more evident. In Nuc, as explained by Stuckey and Dixon [26], two identical monomers associate together where one histidine assumes the role of the nucleophile and the other the role of the GA/GB in a yet unexplained manner. Since these are identical protein units, with the equivalent environment around both histidines, it seems quite likely that factors such as substrate binding or unit association may trigger local changes in the environment of the active site to induce one of the histidine residues to become the activated nucleophile and the other to become the GA/GB. This hypothesis has been experimentally verified for another homodimeric nuclease belonging to the PLD superfamily, BfiI. The monomer of BfiI contains the recognition site binding domain that guides the enzyme to its target sequence and the phosphodiesterase domain that carries out the catalytic activity. In a series of experiments utilising the combination of mutant and WT BfiI monomers, the authors demonstrated that upon binding to the two recognition sites, the situation where the enzyme shows optimal activity, histidine residues belonging to different units of the homodimer actually switch their roles from one DNA molecule to another, while the roles are retained during the cleavage of the top and bottom strand of the same DNA molecule [31].

In the monomeric enzymes like SaPLD and tyrosyl-DNA phosphodiesterase (Tdp1), the HKD motif appears twice in the sequence and its residues form a symmetrical or nearly symmetrical active site. In *Streptomyces* PLD, the active site shows a high degree of symmetry in sequence and arrangement of the crucial residues for catalysis [22]. This symmetry is slightly disturbed in Tdp1 since the C-terminal histidine is coordinated by glutamine while the N-terminal one is coordinated by glutamate [32]. This change in the local environment around the histidines may facilitate the role distribution. Namely, acidic glutamate helps to stabilise the positive charge on the N-terminal histidine and increases its nucleophilicity much more so than the glutamine on the C-terminal histidine. As a result, the N-terminal histidine assumes the role of a nucleophile. In SaPLD such asymmetry is not observed, allowing the hypothesis of the possible role exchange between the catalytic histidines depending on the substrate and its binding mode. Since this study observed a changed behaviour in the mutant SaPLD co-crystalised with its product analogue, further research is needed to understand whether this also occurs naturally, with the WT PLD acting on its natural substrates.

The observed plasticity of SaPLD in this study as well as the above mentioned PLD superfamily members, adds to a growing body of knowledge on enzyme plasticity and catalytic promiscuity in general (reviewed in [33–36]). A few examples include the alkaline phosphatase superfamily [37–39] and the motor domain of myosin [40]. Indeed, examples of enzyme promiscuity brings into question the classic ideas that enzyme active sites are designed to carry out specific chemistry via a single unique mechanism. Enzyme plasticity, by adjusting the roles of different active site residues, provides opportunities for catalytic promiscuity in these complex macromolecules which broadens the scope of enzymatic chemistry and mechanism, as well as enzyme engineering.

Our findings have revealed and explained the novel mode of substrate binding in TNYR SaPLD capable of accepting bulky alcohols such as *myo*-inositol and catalysing the synthesis of 1-PI with high positional specificity. Additionally, we have discovered unexpected plasticity of the TNYR's active site, specifically the possibility of role exchange between the catalytic histidine residues, which are currently considered to be predetermined and fixed. Although further research is needed to elucidate whether the role exchange occurs with the WT enzymes and their natural substrates, we believe that our findings lay an important foundation for further progress in this area of research.

Biochemical Journal (2021) **478** 1749–1767
https://doi.org/10.1042/BCJ20210117

Data Availability

The coordinates and structure factors for all seven structures have been deposited to the PDB. The PDB codes for each structure are as follows: unbound SaPLD TNYR mutant — 7JRB, phosphate bound SaPLD TNYR mutant — 7JRC, the 30 min soak of diC_4PC bound to SaPLD TNYR mutant — 7JRV, the 8 h soak of diC_4PC bound to SaPLD TNYR mutant — 7JRU, the 5 day soak of diC_4PC bound to SaPLD TNYR mutant — 7JRW, the 1-inositol phosphate soak of the inactive (H168A) SaPLD TNYR mutant — 7JS5 and the 1-inositol phosphate co-crystal of SaPLD TNYR mutant — 7JS7.

Competing Interests

The authors declare that there are no competing interests associated with the manuscript.

Funding

The authors acknowledge funding support from the University of Western Australia in the form of a Research Collaboration Award.

CRediT Author Contribution

Alice Vrielink: Conceptualization, Resources, Formal analysis, Supervision, Funding acquisition, Validation, Writing — original draft, Project administration, Writing — review and editing. **Ariela Samantha:** Formal analysis, Investigation, Writing — original draft. **Jasmina Damnjanović:** Conceptualization, Resources, Formal analysis, Funding acquisition, Writing — review and editing. **Yugo Iwasaki:** Conceptualization, Formal analysis, Funding acquisition, Validation, Writing — review and editing. **Hideo Nakano:** Funding acquisition, Writing — review and editing.

Acknowledgements

The authors thank the Australian Synchrotron for access to X-ray beamtime and beamline support.
A.S. acknowledges the Indonesia Endowment Fund for Education (Lembaga Pengelola Dana Pendidikan) for scholarship funding support.

Abbreviations

CASTp, computed atlas of surface topography of proteins; FPLC, fast performance liquid chromatography; HKD, HxKxxxxDx6GSxN; LDAO, lauryldimethylamine *N*-oxide; MES, *N*-morpholinoethanesulfonic acid; PA, phosphatidic acid; PI, phosphatidylinositol; PLD, Phospholipase D; PLs, Phospholipids.

References

1 Guo, Z., Vikbjerg, A.F. and Xu, X. (2005) Enzymatic modification of phospholipids for functional applications and human nutrition. *Biotechnol. Adv.* **23**, 203–259 https://doi.org/10.1016/j.biotechadv.2005.02.001
2 Li, J., Wang, X., Zhang, T., Wang, C., Huang, Z., Luo, X. et al. (2015) A review on phospholipids and their main applications in drug delivery systems. *Asian J. Pharm. Sci.* **10**, 81–98 https://doi.org/10.1016/j.ajps.2014.09.004
3 Borrelli, G. and Trono, D. (2015) Recombinant lipases and phospholipases and their use as biocatalysts for industrial applications. *Int. J. Mol. Sci.* **16**, 20774–20840 https://doi.org/10.3390/ijms160920774
4 Bruzik, K. and Tsai, M.D. (1982) Phospholipids chiral at phosphorus .1. Stereochemistry of transphosphatidylation catalyzed by phospholipase-D. *J. Am. Chem. Soc.* **104**, 863–865 https://doi.org/10.1021/ja00367a044
5 Bruzik, K. and Tsai, M.D. (1984) Phospholipids chiral at phosphorus. Synthesis of chiral phosphatidylcholine and stereochemistry of phospholipase D. *Biochemistry* **23**, 1656–1661 https://doi.org/10.1021/bi00303a012
6 Selvy, P.E., Lavieri, R.R., Lindsley, C.W. and Brown, H.A. (2011) Phospholipase D: enzymology, functionality, and chemical modulation. *Chem. Rev.* **111**, 6064–6119 https://doi.org/10.1021/cr200296t
7 Uesugi, Y. and Hatanaka, T. (2009) Phospholipase D mechanism using streptomyces PLD. *Biochim. Biophys. Acta* **1791**, 962–969 https://doi.org/10.1016/j.bbalip.2009.01.020
8 Ulbrich-Hofmann, R., Lerchner, A., Oblozinsky, M. and Bezakova, L. (2005) Phospholipase D and its application in biocatalysis. *Biotechnol. Lett.* **27**, 535–544 https://doi.org/10.1007/s10529-005-3251-2
9 Damnjanović, J. and Iwasaki, Y. (2013) Phospholipase D as a catalyst: application in phospholipid synthesis, molecular structure and protein engineering. *J. Biosci. Bioeng.* **116**, 271–280 https://doi.org/10.1016/j.jbiosc.2013.03.008

10 Masayama, A., Takahashi, T., Tsukada, K., Nishikawa, S., Takahashi, R., Adachi, M. et al. (2008) Streptomyces phospholipase D mutants with altered substrate specificity capable of phosphatidylinositol synthesis. *ChemBioChem* **9**, 974–981 https://doi.org/10.1002/cbic.200700528
11 Masayama, A., Tsukada, K., Ikeda, C., Nakano, H. and Iwasaki, Y. (2009) Isolation of phospholipase D mutants having phosphatidylinositol-synthesizing activity with positional specificity on *myo*-inositol. *ChemBioChem* **10**, 559–564 https://doi.org/10.1002/cbic.200800651
12 Damnjanović, J., Kuroiwa, C., Tanaka, H., Ishida, K., Nakano, H. and Iwasaki, Y. (2016) Directing positional specificity in enzymatic synthesis of bioactive 1-phosphatidylinositol by protein engineering of a phospholipase D. *Biotechnol. Bioeng.* **113**, 62–71 https://doi.org/10.1002/bit.25697
13 Iwasaki, Y., Masayama, A., Mori, A., Ikeda, C. and Nakano, H. (2009) Composition analysis of positional isomers of phosphatidylinositol by high-performance liquid chromatography. *J. Chromatogr. A* **1216**, 6077–6080 https://doi.org/10.1016/j.chroma.2009.06.064
14 Damnjanovic, J., Matsunaga, N., Adachi, M., Nakano, H. and Iwasaki, Y. (2018) Facile enzymatic synthesis of phosphatidylthreonine using an engineered phospholipase D. *Eur. J. Lipid Sci. Technol.* **120**, 1800089 https://doi.org/10.1002/ejlt.201800089
15 Inoue, A., Adachi, M., Damnjanović, J., Nakano, H. and Iwasaki, Y. (2016) Direct enzymatic synthesis of 1-Phosphatidyl-β-D-glucose by engineered phospholipase D. *ChemistrySelect* **1**, 4121–4125 https://doi.org/10.1002/slct.201600839
16 Iwasaki, Y., Mishima, N., Mizumoto, K., Nakano, H. and Yamane, T. (1995) Extracellular production of phospholipase D of *Streptomyces antibioticus* using recombinant *escherichia coli*. *J. Ferment. Bioeng.* **79**, 417–421 https://doi.org/10.1016/0922-338X(95)91254-3
17 Studier, F.W. (2005) Protein production by auto-induction in high-density shaking cultures. *Protein Expr. Purif.* **41**, 207–234 https://doi.org/10.1016/j.pep.2005.01.016
18 Iwasaki, Y., Tsubouchi, Y., Ichihashi, A., Nakano, H., Kobayashi, T., Ikezawa, H. et al. (1998) Two distinct phosphatidylinositol-specific phospholipase Cs from *Streptomyces antibioticus*. *Biochim Biophys Acta* **1391**, 52–66 https://doi.org/10.1016/S0005-2760(97)00191-4
19 Kabsch, W. (2010) XDS. *Acta Crystallogr. D Biol. Crystallogr.* **66**, 125–132 https://doi.org/10.1107/S0907444909047337
20 Winn, M.D., Ballard, C.C., Cowtan, K.D., Dodson, E.J., Emsley, P., Evans, P.R. et al. (2011) Overview of the CCP4 suite and current developments. *Acta Crystallogr. D Biol. Crystallogr.* **67**, 235–242 https://doi.org/10.1107/S0907444910045749
21 Suzuki, A., Kakuno, K., Iwasaki, Y., Yamane, T. and Yamane, T. (1999) Crystallization and preliminary X-ray diffraction studies of phospholipase D from *Streptomyces antibioticus*. *Acta Crystallogr. D Biol. Crystallogr.* **55**, 317–319 https://doi.org/10.1107/S0907444998010592
22 Leiros, I., McSweeney, S. and Hough, E. (2004) The reaction mechanism of phospholipase D from *Streptomyces* sp. strain PMF. Snapshots along the reaction pathway reveal a pentacoordinate reaction intermediate and an unexpected final product. *J. Mol. Biol.* **339**, 805–820 https://doi.org/10.1016/j.jmb.2004.04.003
23 Leiros, I., Secundo, F., Zambonelli, C., Servi, S. and Hough, E. (2000) The first crystal structure of a phospholipase D. *Structure* **8**, 655–667 https://doi.org/10.1016/S0969-2126(00)00150-7
24 Tian, W., Chen, C., Lei, X., Zhao, J. and Liang, J. (2018) CASTp 3.0: Computed atlas of surface topography of proteins. *Nucleic Acids Res.* **46**, W363–W367 https://doi.org/10.1093/nar/gky473
25 Liebschner, D., Afonine, P.V., Moriarty, N.W., Poon, B.K., Sobolev, O.V., Terwilliger, T.C. et al. (2017) Polder maps: improving OMIT maps by excluding bulk solvent. *Acta Crystallogr. D Biol. Crystallogr.* **73**, 148–157 https://doi.org/10.1107/S2059798316018210
26 Stuckey, J.A. and Dixon, J.E. (1999) Crystal structure of a phospholipase D family member. *Nat. Struct. Biol.* **6**, 278–284 https://doi.org/10.1038/6716
27 Djinovic-Carugo, K. and Carugo, O. (2015) Missing strings of residues in protein crystal structures. *Intrinsically Disord. Proteins* **3**, e1095697 https://doi.org/10.1080/21690707.2015.1095697
28 Yao, S. and Moseley, H.N.B. (2020) A chemical interpretation of protein electron density maps in the worldwide protein data bank. *PLoS ONE* **15**, e0236894 https://doi.org/10.1371/journal.pone.0236894
29 Negishi, T., Mukaihara, T., Mori, K., Nishikido, H., Kawasaki, Y., Aoki, H. et al. (2005) Identification of a key amino acid residue of streptomyces phospholipase D for thermostability by in vivo DNA shuffling. *Biochim. Biophys. Acta* **1722**, 331–342 https://doi.org/10.1016/j.bbagen.2005.01.009
30 Iwasaki, Y., Horiike, S., Matsushima, K. and Yamane, T. (1999) Location of the catalytic nucleophile of phospholipase D of Streptomyces antibioticus in the C-terminal half domain. *Eur. J. Biochem.* **264**, 577–581 https://doi.org/10.1046/j.1432-1327.1999.00669.x
31 Sasnauskas, G., Zakrys, L., Zaremba, M., Cosstick, R., Gaynor, J.W., Halford, S.E. et al. (2010) A novel mechanism for the scission of double-stranded DNA: BfiI cuts both 3′–5′ and 5′–3′ strands by rotating a single active site. *Nucleic Acids Res.* **38**, 2399–2410 https://doi.org/10.1093/nar/gkp1194
32 Davies, D.R., Interthal, H., Champoux, J.J. and Hol, W.G. (2002) The crystal structure of human tyrosyl-DNA phosphodiesterase, Tdp1. *Structure* **10**, 237–248 https://doi.org/10.1016/S0969-2126(02)00707-4
33 Bornscheuer, U.T. and Kazlauskas, R.J. (2004) Catalytic promiscuity in biocatalysis: using old enzymes to form new bonds and follow new pathways. *Angew. Chem. Int. Ed. Engl.* **43**, 6032–6040 https://doi.org/10.1002/anie.200460416
34 Khersonsky, O. and Tawfik, D.S. (2010) Enzyme promiscuity: a mechanistic and evolutionary perspective. *Annu. Rev. Biochem.* **79**, 471–505 https://doi.org/10.1146/annurev-biochem-030409-143718
35 O'Brien, P.J. and Herschlag, D. (1999) Catalytic promiscuity and the evolution of new enzymatic activities. *Chem. Biol.* **6**, R91–R105 https://doi.org/10.1016/S1074-5521(99)80033-7
36 Pabis, A. and Kamerlin, S.C. (2016) Promiscuity and electrostatic flexibility in the alkaline phosphatase superfamily. *Curr. Opin. Struct. Biol.* **37**, 14–21 https://doi.org/10.1016/j.sbi.2015.11.008
37 Hou, G. and Cui, Q. (2012) QM/MM analysis suggests that alkaline phosphatase (AP) and nucleotide pyrophosphatase/phosphodiesterase slightly tighten the transition state for phosphate diester hydrolysis relative to solution: implication for catalytic promiscuity in the AP superfamily. *J. Am. Chem. Soc.* **134**, 229–246 https://doi.org/10.1021/ja205226d
38 Hou, G. and Cui, Q. (2013) Stabilization of different types of transition states in a single enzyme active site: QM/MM analysis of enzymes in the alkaline phosphatase superfamily. *J. Am. Chem. Soc.* **135**, 10457–10469 https://doi.org/10.1021/ja403293d
39 Roston, D., Demapan, D. and Cui, Q. (2016) Leaving group ability observably affects transition state structure in a single enzyme active site. *J. Am. Chem. Soc.* **138**, 7386–7394 https://doi.org/10.1021/jacs.6b03156
40 Lu, X., Ovchinnikov, V., Demapan, D., Roston, D. and Cui, Q. (2017) Regulation and plasticity of catalysis in enzymes: insights from analysis of mechanochemical coupling in myosin. *Biochemistry* **56**, 1482–1497 https://doi.org/10.1021/acs.biochem.7b00016